Atmospheric Flight Gust Loads Analysis

July 1999

Prepared by

M. C. KIM, A. M. KABE, S. S. LEE
Structural Dynamics Department

Prepared for

SPACE AND MISSILE SYSTEMS CENTER
AIR FORCE MATERIEL COMMAND
2430 E. El Segundo Boulevard
Los Angeles Air Force Base, CA 90245

Engineering and Technology Group

THE AEROSPACE
CORPORATION
El Segundo, California

20000824 081

Maj. Charles R. Williamson
Project Officer

REPORT DOCUMENTATION PAGE

Form Approved
OMB No. 0704-0188

1. AGENCY USE ONLY (Leave blank)	2. REPORT DATE	3. REPORT TYPE AND DATES COVERED
	July 1999	Final

4. TITLE AND SUBTITLE	5. FUNDING NUMBERS
Atmospheric Flight Gust Loads Analysis	F04701-93-C-0094

6. AUTHOR(S)

M. C. Kim, A. M. Kabe, S. S. Lee

7. PERFORMING ORGANIZATION NAME(S) AND ADDRESS(ES)	8. PERFORMING ORGANIZATION REPORT NUMBER
The Aerospace Corporation 2350 E. El Segundo Boulevard El Segundo, CA 90245	TR-99(1534)-5

9. SPONSORING/MONITORING AGENCY NAME(S) AND ADDRESS(ES)	10. SPONSORING/MONITORING AGENCY REPORT NUMBER
Space and Missile Systems Center Air Force Materiel Command 2430 E. El Segundo Boulevard Los Angeles Air Force Base, CA 90245	SMC-TR-00-24

11. SUPPLEMENTARY NOTES

12a. DISTRIBUTION/AVAILABILITY STATEMENT	12b. DISTRIBUTION CODE
Approved for public release; distribution unlimited	

13. ABSTRACT (Maximum 200 words)

A new Monte Carlo atmospheric flight gust loads analysis approach is presented. The procedure uses forcing functions that were derived by extracting the turbulent, short-duration, non-persistent components of measured wind profiles. Over 1000 forcing functions were used in each analysis. The results were analyzed statistically to establish the 99.7 percent enclosure, 90 percent confidence level, load values. Results are presented for a medium lift launch vehicle and a heavy lift launch vehicle. Loads for various altitude bands, time of year, and the Eastern Range and Western Range launch facilities in the United States are compared. Also, the Monte Carlo results are compared to a prevalent synthetic gust analysis approach in use today.

14. SUBJECT TERMS Atmospheric flight loads, gust, forcing function, launch vehicle loads, statistical load levels	15. NUMBER OF PAGES 46
	16. PRICE CODE

17. SECURITY CLASSIFICATION OF REPORT	18. SECURITY CLASSIFICATION OF THIS PAGE	19. SECURITY CLASSIFICATION OF ABSTRACT	20. LIMITATION OF ABSTRACT
Unclassified	Unclassified	Unclassified	

Abstract

A new Monte Carlo atmospheric flight gust loads analysis approach is presented. The procedure uses forcing functions that were derived by extracting the short-duration, turbulent components of measured wind profiles. Over 1000 forcing functions were used in each analysis. The load analysis results were analyzed statistically to establish the 99.7 percent enclosure, 90 percent confidence level, load values. Results are presented for a medium lift launch vehicle and a heavy lift launch vehicle. Loads for various altitude bands, time of year, and the Eastern Range and Western Range launch facilities in the United States are compared. Also, the Monte Carlo results are compared to a prevalent synthetic gust analysis approach in use today.

1

Contents

Figures

Table

Acknowledgments

Nomenclature

C aerodynamic force coefficients, dimensionless

$[C_p']$ system diagonal matrix of partial derivatives of C with respect to angle of attack, rad^{-1}

f_G gust frequency, Hz

$\{f(t)\}$ vector of system external force, lbf

$\{\bar{f}(t)\}$ vector of system external force other than wind forces, lbf

$[I]$ system modal mass matrix, lbm

$[N]$ system aerodynamic stiffness matrix, lbf/rad

$[\dot{N}]$ system aerodynamic damping matrix, lbf-s/in

Q dynamic pressure, lbf/in^2

$\{q(t)\}$ vector of system generalized coordinates

S reference area, in^2

t independent time variable

v velocity, ft/sec

$\dot{z}(t)$ velocity in the direction of z axis, in/s

$\alpha(t)$ total angle of attack in the pitch plane, rad

$\{\Gamma_p\}$ aerodynamic force vector, lbf/rad

$[2\varsigma\omega]$ system generalized damping matrix, lbf-s/in

$\{\theta(t)\}$ rotation, rad

λ gust wavelength, ft

$[\Phi]$ system modal matrix, dimensionless

$[\omega^2]$ system modal stiffness matrix, lbf/in and lbf/rad

Superscripts

T transposed

Subscripts

f forced

G gust

j degree-of-freedom number

p pitch plane

RW relative wind

r rotation

t translation

y y axis

z z axis

1. Introduction

During atmospheric flight a launch vehicle and its payload will experience severe structural loading from several different sources. Among the more critical is atmospheric turbulence. Analyses performed to establish launch and space vehicle atmospheric turbulence loads are generally referred to as gust loads analyses.

As early as 1964, Refs. 1 and 2 suggested that the detailed characteristics of measured wind profiles be used to establish the response of launch vehicles to turbulence. References 3 and 4 also made similar suggestions. However, because of computational considerations, launch vehicle gust loads analyses have generally involved the use of synthetic gust profiles whose properties were established from aircraft response data[5-8] or wind profile measurements.[9-13] Reference 4 addressed the issue of whether gusts derived from horizontally flying aircraft could be applied to a rising launch vehicle. Treddenick[14] compared aircraft-derived data to that obtained with vertically rising Jimsphere balloons and concluded that the aircraft data was more severe.

The two most common synthetic profiles used today are the one-minus-cosine profile[15] and the one-minus-cosine with a flattop profile.[16,17] Other profiles that have been suggested, and/or used, include sharp-edged and linear-ramp profiles,[18,19] triangular, trapezoidal, and sine profiles (Ref. 4) and a Z-shaped profile.[20] The appendix contains a detailed description and comparison of the two most prevalent profiles in use today.

Inherent in the synthetic gust profile approach is the assumption that the synthetic profiles will yield loads that are equivalent to some level of statistical conservatism that would be obtained if a launch vehicle was subjected to a large number of the actual wind profiles. However, no analyses have been performed, to date, that compare loads obtained with synthetic profiles to loads obtained with a large number of measured turbulence profiles.

The purpose of this paper is to introduce a Monte Carlo gust loads analysis approach that uses the turbulent components of measured wind profiles as forcing functions, and establishes loads of a desired statistical level. This paper describes the actual gust loads analyses and compares the results to loads obtained with the most widely used synthetic profile approach.

2. New Gust Loads Analysis Procedure

Figure 1 shows a top-level outline of the Monte Carlo gust loads analysis procedure. The main steps will be summarized in this section, and discussed in more detail in subsequent sections. The first step was to develop two large families of gust forcing functions—one for the Eastern Range (ER) of the United States, located in Florida, and one for the Western Range (WR) of the United States, located in California.[21,22] Next, gust loads analyses were performed using each of the new forcing functions. The solution procedure was identical to that used with the synthetic profiles, except that instead of using a one-minus-cosine profile, actual wind profiles were used. Finally, for each load parameter of interest, the peak value obtained with each forcing function was included in a statistical analysis[23] to establish the 99.7 percent enclosure, 90 percent confidence level, load value.
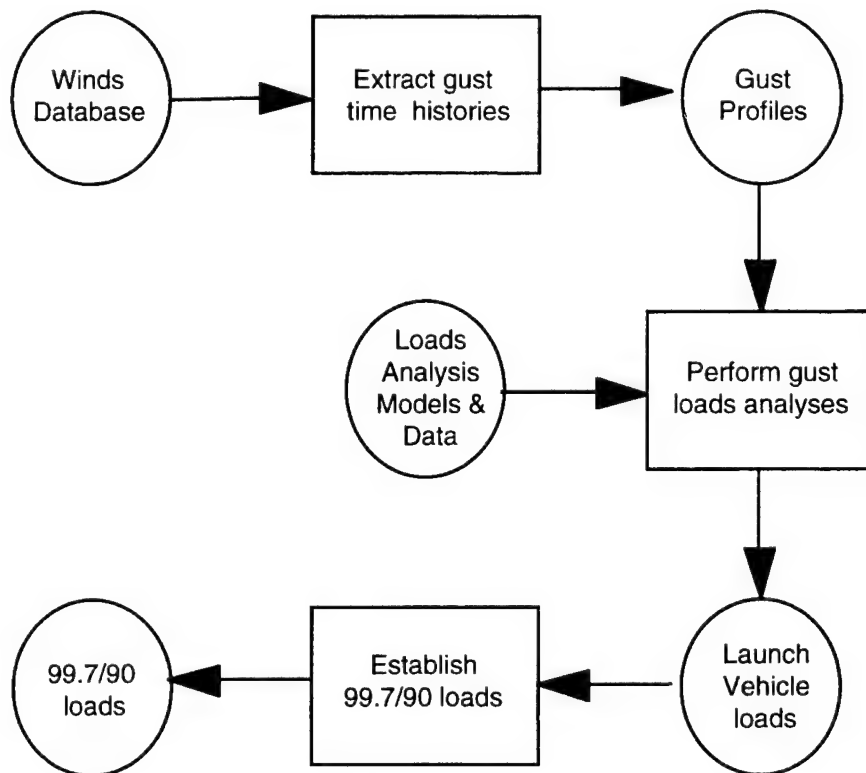
Figure 1. Overview of Monte Carlo gust loads analysis approach. Significant differences from current approaches include the use of measured wind profiles to develop empirical gust forcing functions and the use of distribution-free statistics to develop the desired statistical load level.

3. Turbulence/Gust Forcing Functions

The turbulence/gust profiles were developed from a large number of measured wind velocity (magnitude and direction) profiles obtained with Jimsphere balloons (Ref. 22). Most were associated with day-of-launch operations. The WR winds database contained 1093 profiles, and the ER database contained 1197 profiles.

The first step in developing the forcing functions was to establish the wavelength that represented the boundary between the slowly-varying wind components and the short-duration, non-persistent components (Ref. 21). This boundary is a function of time between when a wind is measured and a launch vehicle flies through it. By removing from a measured profile the longer, more persistent wavelengths, one is left with the short-duration, turbulent components. Because turbulence changes fairly rapidly with time, loads due to this portion of the wind need to be treated statistically.

Once the slowly-varying portion was removed, profiles corresponding to 6,000 ft of altitude were extracted, and the ends were tapered to avoid step inputs. It should also be noted that for the purposes of this study, the forcing functions were developed from the magnitude of the measured wind, without considering the wind direction and its relationship to the launch vehicle flight axis or azimuth. For each altitude band of interest, over 1000 forcing functions were developed for each launch range. Complete details of the forcing function development are presented in Ref. 22. Figure 2 presents a typical profile. Forcing functions were developed for the 32000-38000 ft, 36000-42000 ft, 38000-44000 ft, and 42000-48000 ft altitude bands.

Figure 2. Example of turbulent component of Jimsphere balloon data.

4. Equations of Motion

The gust loads analyses were performed with the same assumptions as used with the synthetic profile approach. The turbulence/gust was assumed to act normal to the launch vehicle longitudinal axis and, thus, it represented a time-varying deviation from the relatively small vehicle angle of attack due to the ve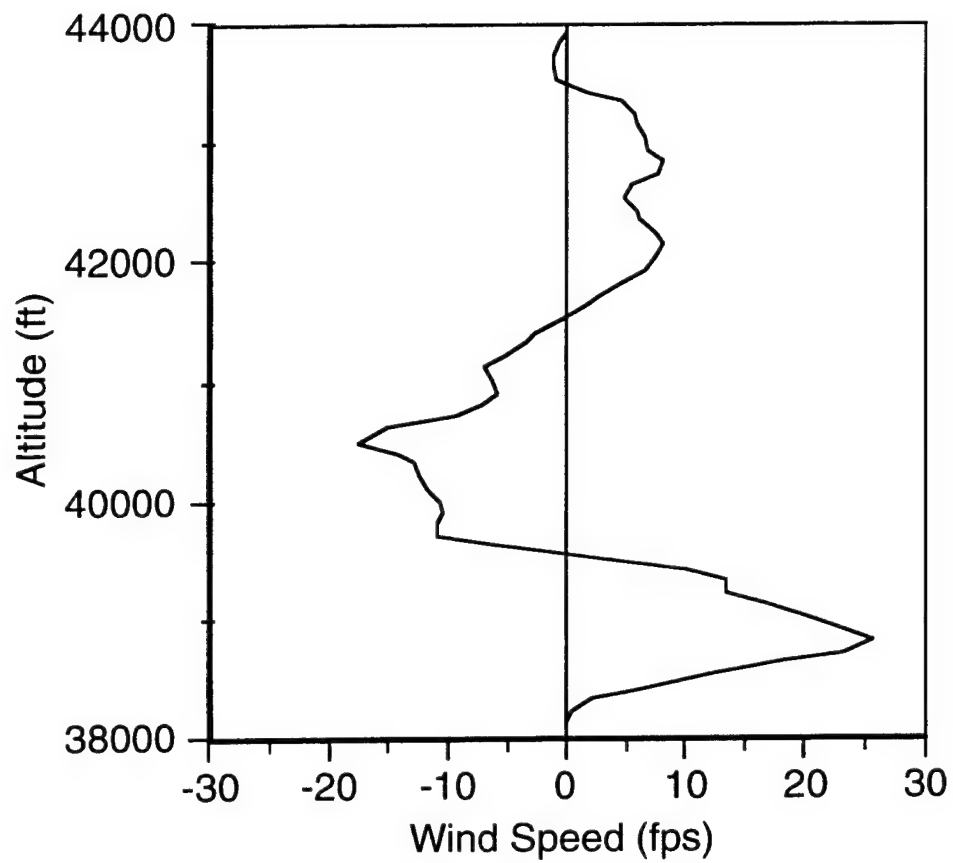hicle's motion through the air. It was also assumed that the launch vehicle was immersed in the turbulence/gusts instantaneously. Therefore, the turbulence/gust velocity profile became a time-dependent modulation of the local angle of attack along the length of the vehicle. Experience indicates that launch vehicle structural dynamic and aerodynamic properties do not vary significantly during the 6,000-ft altitude bands used in the analyses and, thus, a model with fixed parameters was used.

The dynamic models were developed by component mode coupling the launch and space vehicle models. The equations of motion obtained, in generalized coordinates, can be written in matrix notation as

$$[I]\{\ddot{q}(t)\} + [2\varsigma\omega]\{\dot{q}(t)\} + [\omega^2]\{q(t)\} = [\Phi]^T_f \{f(t)\} \tag{1}$$

and where $[\Phi]_f$ is the modal matrix that transforms the forced physical degrees of freedom (DOF) of the launch vehicle model to generalized coordinates.

To facilitate the presentation, only the pitch plane equations will be presented. The yaw plane equations were derived in a similar fashion, and no coupling between the two planes was assumed. In the launch vehicle coordinate system, the aerodynamic forces at the j th degree of freedom, pitch plane, can be defined as

$$f_j(t) = QS \left(\frac{\partial C_p}{\partial \alpha} \right)_j \alpha_j(t) \tag{2}$$

where the total angle of attack at the j th degree of freedom is given by

$$\alpha_j(t) = \frac{v(t)}{v_{RW}} - \frac{\dot{z}_j(t)}{v_{RW}} + \theta_{y,j}(t) \tag{3}$$

The aerodynamic normal force coefficients, Cp, for the vehicles considered in this paper, were derived from wind tunnel test data. By substituting Eq. (3) into Eq. (2), we obtain

$$\{f_p(t)\} = QS [C_p'] \left(\{I\} \frac{v(t)}{v_{RW}} - \{ \frac{\dot{z}(t)}{v_{RW}} \} + \{\theta_y(t)\} \right) \tag{4}$$

Substituting Eq. (4) into Eq. (1) yields

$$[I]\{\ddot{q}(t)\} + \left([2\varsigma\omega] + [\dot{N}p]\right)\{\dot{q}(t)\} + \left([\omega^2] + [N_p]\right)\{q(t)\} = \{\Gamma_p\}\frac{v(t)}{v_{RW}} + [\Phi]_f^T\{\bar{f}(t)\} \tag{5}$$

and where the aerodynamic damping, $[\dot{N}_p]$, aerodynamic stiffness, $[N_p]$, and generalized pitch gust force, $\{\Gamma_p\}$, are given by

$$[\dot{N}p] = -\frac{QS}{v_{RW}}[\Phi_{tz}]^T[C_p'][\Phi_{tz}] \tag{6}$$

$$[N_p] = QS[\Phi_{tz}]^T[C_p'][\Phi_{ry}] \tag{7}$$

$$\{\Gamma_p\} = QS[\Phi_{tz}]^T[C_p']\{I\} \tag{8}$$

The specific signs for the aerodynamic damping and stiffness depend on the dynamic model and the aerodynamic force coordinate systems. The formulation in Eqs. (2)-(8) is used by a number of organizations performing launch vehicle gust loads analyses.

5. Response Calculations

Equation 5 was augmented with an autopilot simulation. The equations of motion, which included modes to 20 Hz, the aerodynamic damping and stiffness properties, and the fully coupled autopilot, were numerically integrated using a fourth-order Runge-Kutta procedure. Each simulation was run for 3.5 sec. of equivalent flight time, and response quantities and loads were recovered with response recovery transformation matrices. For the heavy lift launch vehicle, a total of 125 coupled equations of motion were numerically integrated, and for the medium lift launch vehicle, a total of 61 equations were numerically integrated. Figure 3 shows a typical rate gyro response time history for the medium lift launch vehicle; Fig. 4 shows the corresponding computed engine gimbal angle time history; and, Fig. 5 shows a typical bending moment time history. The peak value from each load time history was recorded, and the analysis was repeated for the next forcing function. Table 1 summarizes the number of gust cases.
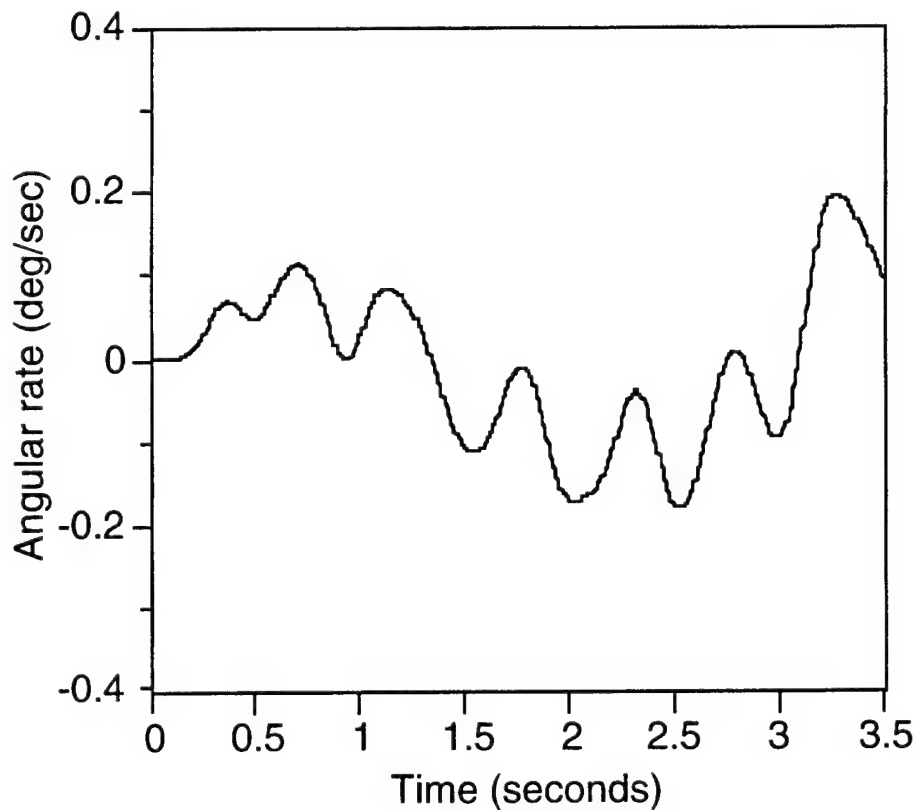
Figure 3. Typical medium lift launch vehicle computed rate gyro response.
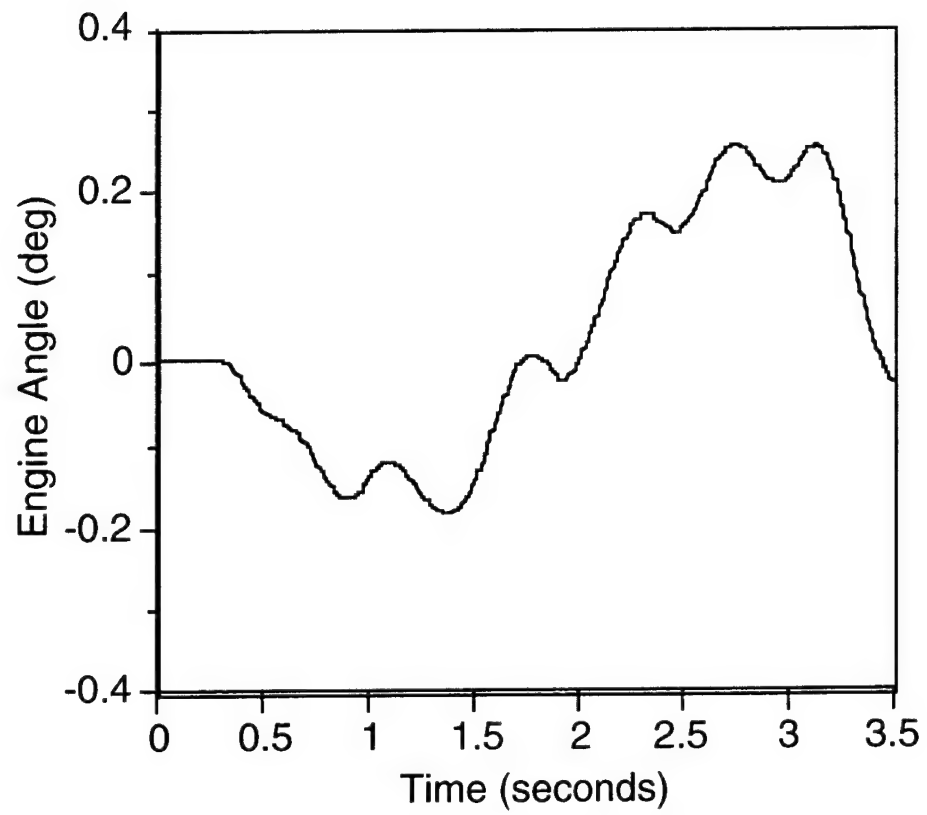
Figure 4. Typical medium lift launch vehicle computed engine gimbal angle response.
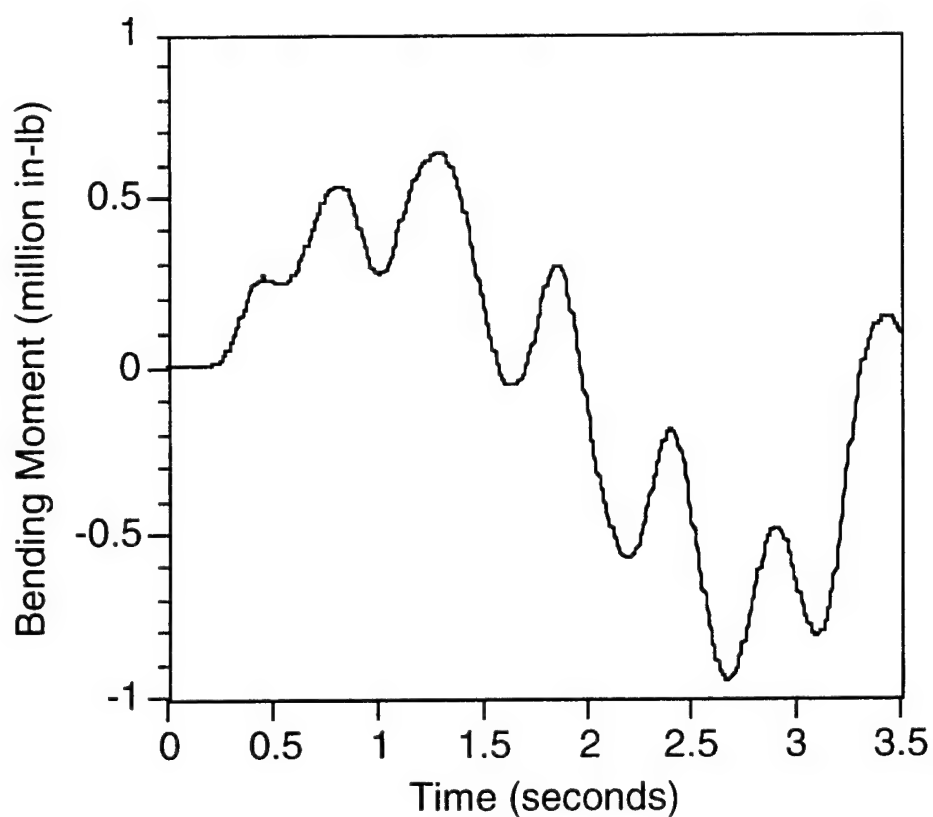
Figure 5. Typical medium lift launch vehicle computed bending moment response for peak bending moment station.

Table 1. Number of Gust Cases

Altitude Band (ft)	Persistence Time (min)	WR	ER
	30	1090	1191
32000-38000	45	1090	1190
	60	1090	1190
	30	1060	1190
36000-42000	45	1060	1190
	60	1059	1190
	30	1053	1188
38000-44000	45	1053	1188
	60	1053	1189
	30	1040	1176
42000-48000	45	1040	1175
	60	1040	1176

6. Statistical Analysis of Results

For each altitude band, over 1000 turbulence/gust forcing function profiles were used in the Monte Carlo analysis. From each calculated response time history the peak value was extracted. For each parameter, the peak values were plotted on normal and gamma probability graphs. The data followed a gamma distribution closely. Figure 6 presents a typical histogram of the maximum bending moments obtained for the heavy lift launch vehicle peak bending moment station, and Fig. 7 presents a typical histogram for the medium lift launch vehicle. Reference 23 describes, in detail, the nonparametric approach used to establish the 99.7 percent enclosure, 90 percent confidence level, values for each load parameter. All results presented in this paper, unless otherwise indicated, are 99.7 percent enclosure, 90 percent confidence level, values.

Figure 6. Heavy lift launch vehicle peak pitch bending moment distribution for WR, 38-44k ft altitude band. The data follow a gamma distribution. The mean and the 99.7/90 value obtained with the reference procedure[23] are also shown.

23

Figure 7. Medium lift launch vehicle peak pitch bending moment distribution for WR, 38-44k ft altitude band. The data follow a gamma distribution. The mean and the 99.7/90 value obtained with the reference procedure[23] are also shown.
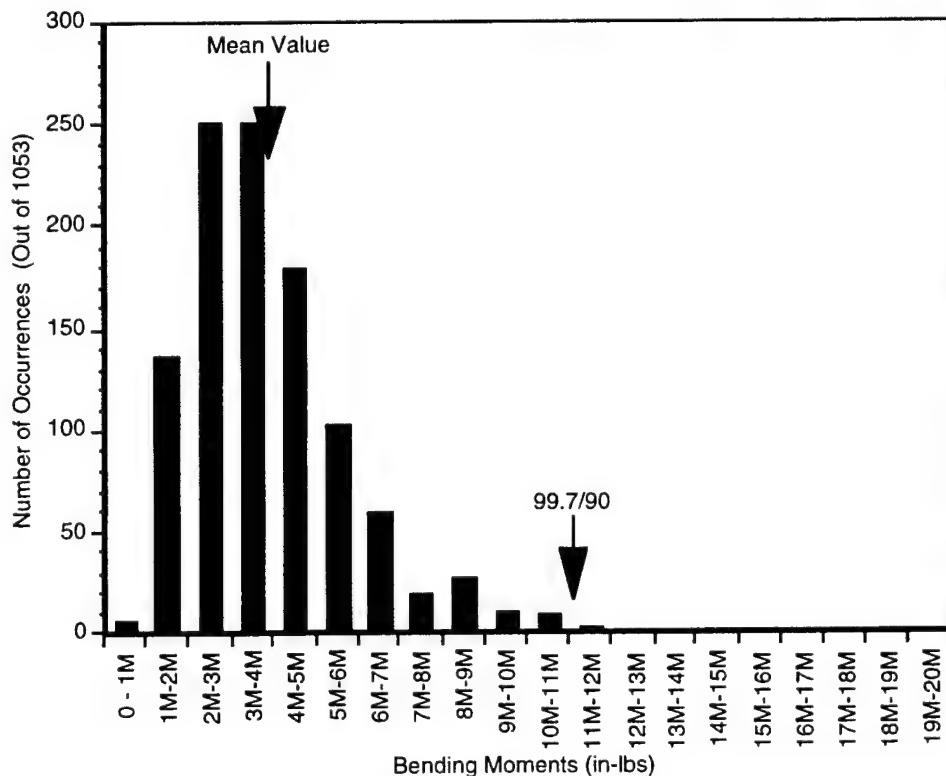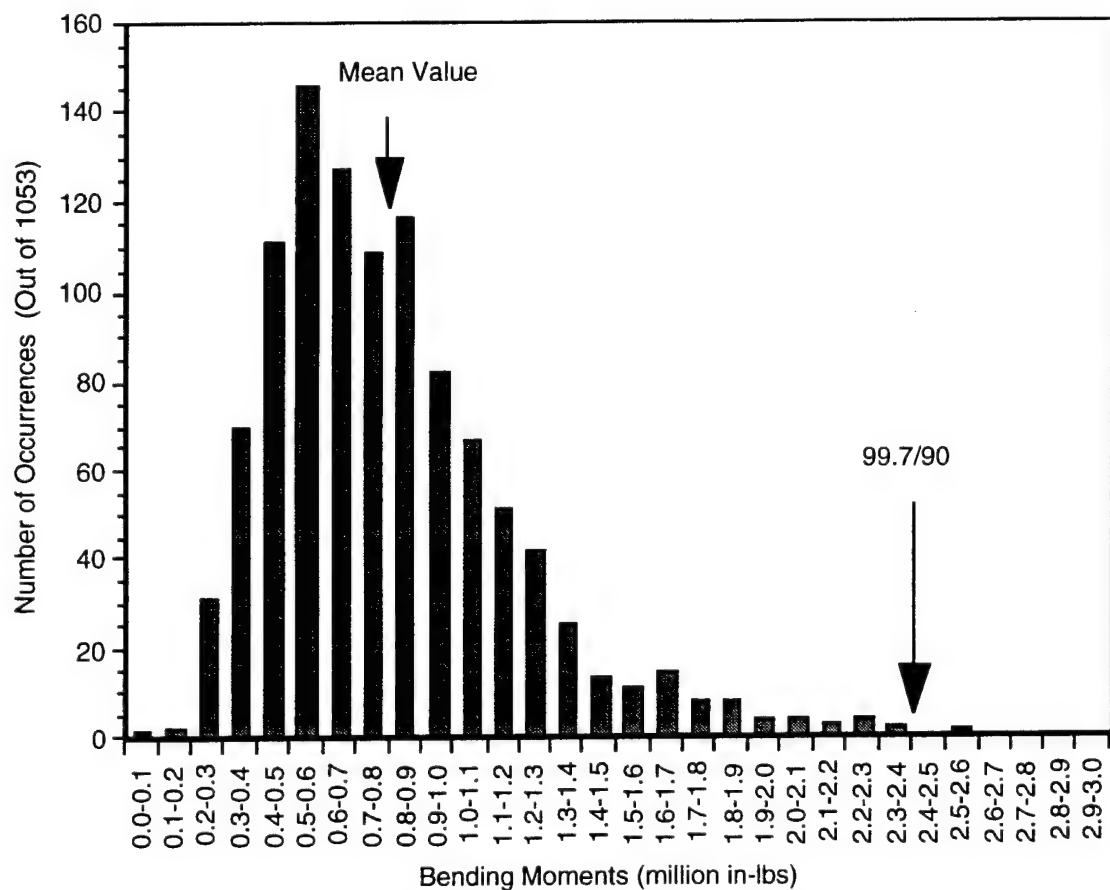
7. Monte Carlo Gust Loads Analysis Results

A number of significant results were obtained from the Monte Carlo study. Each will be described in detail.

7.1 Wind Measurement Time Effects

As discussed in Refs. 21 and 22, the components of wind profiles that need to be considered as turbulent are a function of the difference between the time that the day-of-launch profile is measured and the time that the launch vehicle is launched. The longer the time period, the longer the wavelengths of the components retained in the turbulence/gust profiles must be. The forcing functions developed for this study corresponded to 30-, 45-, and 60-minute time periods.

Figures 8-11 present, for the medium and heavy lift launch vehicles, bending moments for the three time periods discussed above. The values presented are for the 38,000 to 44,000-ft altitude band, which for these vehicles generally yielded the highest loads. Figures 8 and 10 present the results for the Eastern Range, and Figs. 9 and 11 present the results for the Western Range. In these figures, the results obtained for two amplitudes of the 1-cosine synthetic gust profiles are shown with dashed lines.

As can be ascertained from these figures, the loads for the longer time periods are higher. This increase in loads is expected, since the longer time periods correspond to forcing functions that retain longer wavelength wind components. Also, it should be noted that the Western Range results are 10 to 20 percent higher than the Eastern Range. (Also see Figs. 14 and 15.) Thus, one must conclude that turbulence/gust levels are different between the two coasts, with the Western Range being more severe.

In each figure, loads obtained with the one-minus-cosine synthetic profile are also included. In each case the wavelengths of the synthetic profiles were selected such as to coincide with the lower mode periods of vibration. For the medium launch vehicle, several wavelengths up to 1000 ft were used, and for the heavy lift vehicle, several wavelengths up to 1500 ft were used. Two, one-minus-cosine, synthetic gust amplitudes were analyzed—the most widely used value of 30 ft/sec, and a value of 20 ft/sec. As can be ascertained from Figs. 8-11, the 30 ft/sec is more prudent than 20 ft/sec, although not always conservative.

Figure 8. Medium lift launch vehicle pitch bending moment comparison for 30-, 45-, and 60-minute lack-of-wind-persistence times. Eastern Range, 38000-44000 ft altitude band. The data for the 1-cosine synthetic gust profiles are shown in dashed lines.
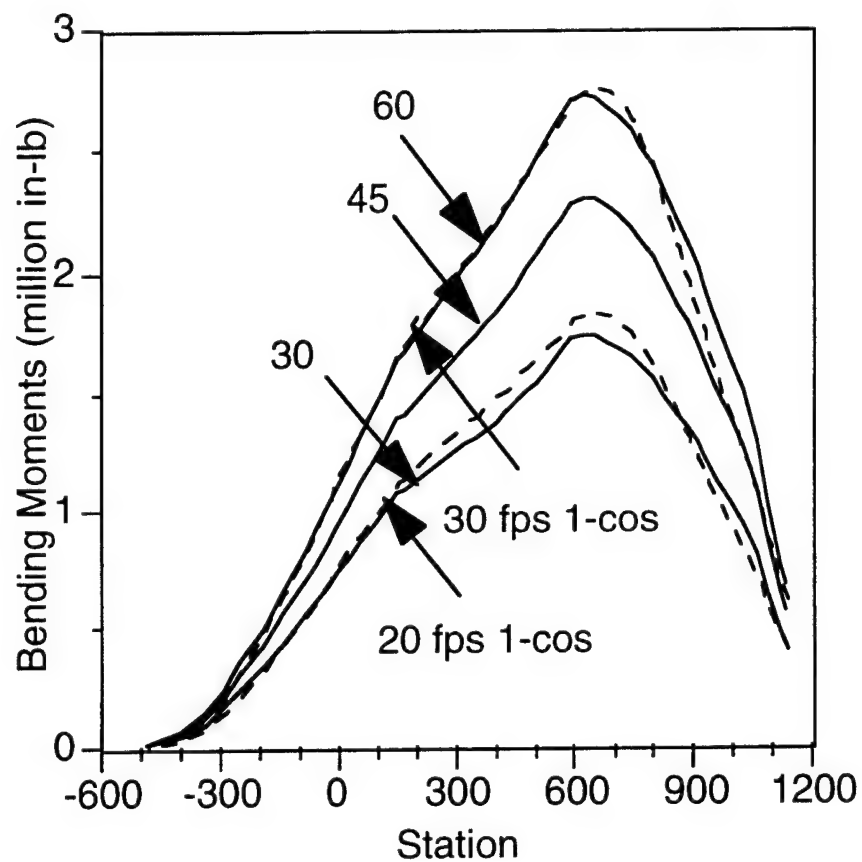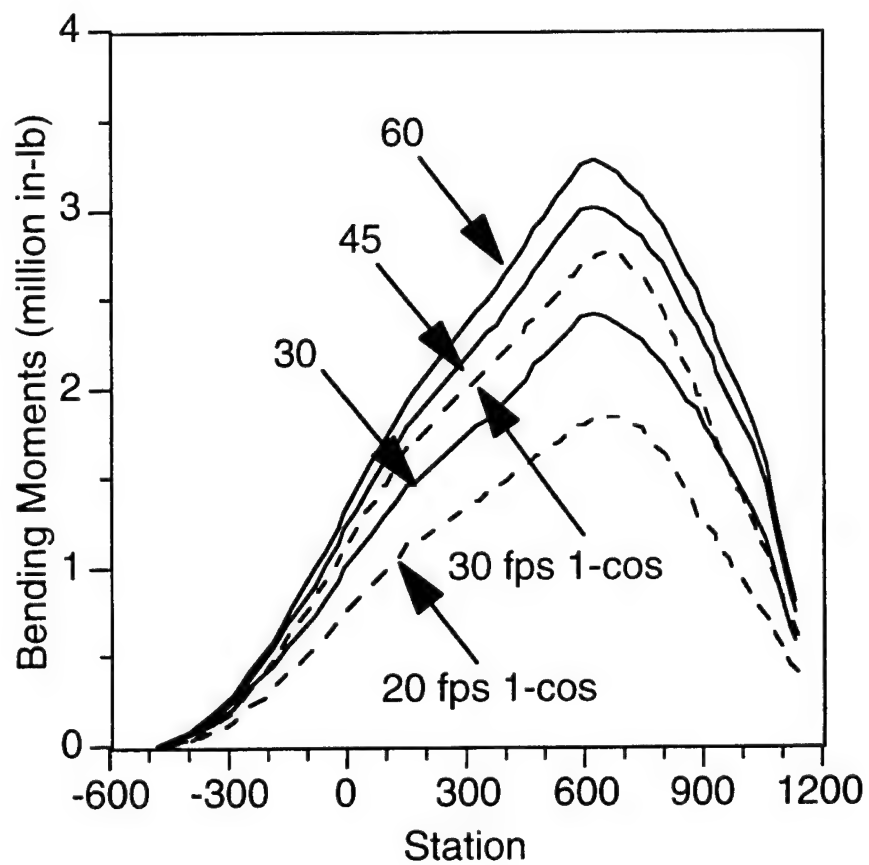
Figure 9.   Medium lift launch vehicle pitch bending moment comparison for 30-,
45-, and 60-minute lack-of-wind-persistence times. Western Range,
38000-44000-ft altitude band.
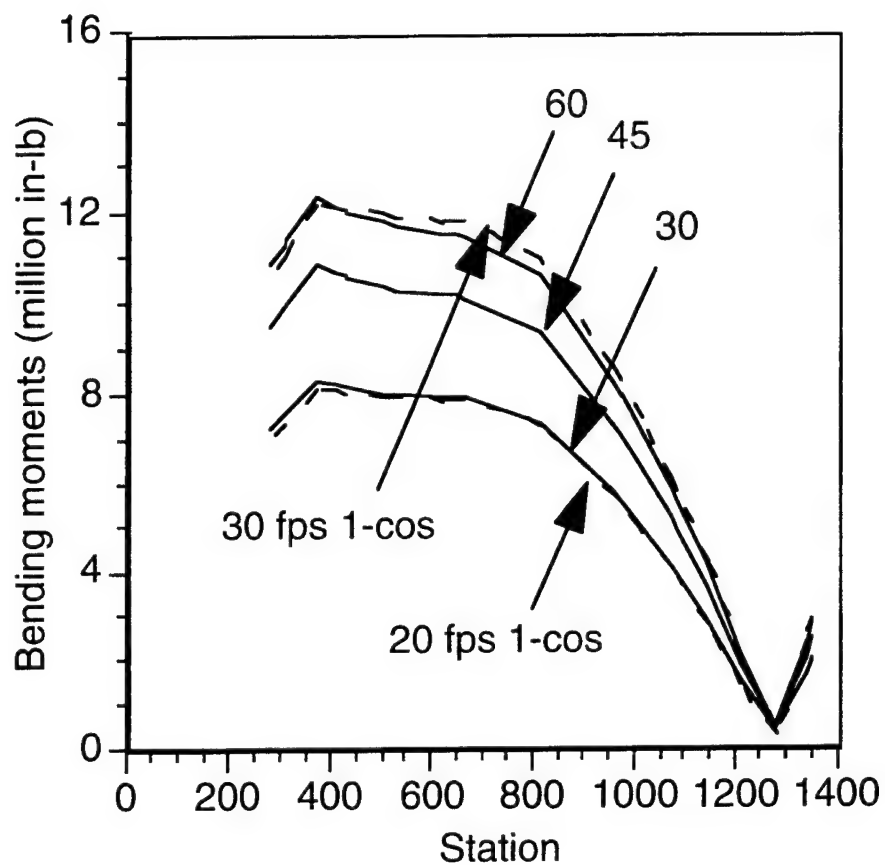
Figure 10. Heavy lift launch vehicle pitch bending moment comparison for stations aft of the payload fairing. Lack-of-wind-persistence times of 30, 45, and 60 minutes. Eastern Range, 38000-44000-ft altitude band.
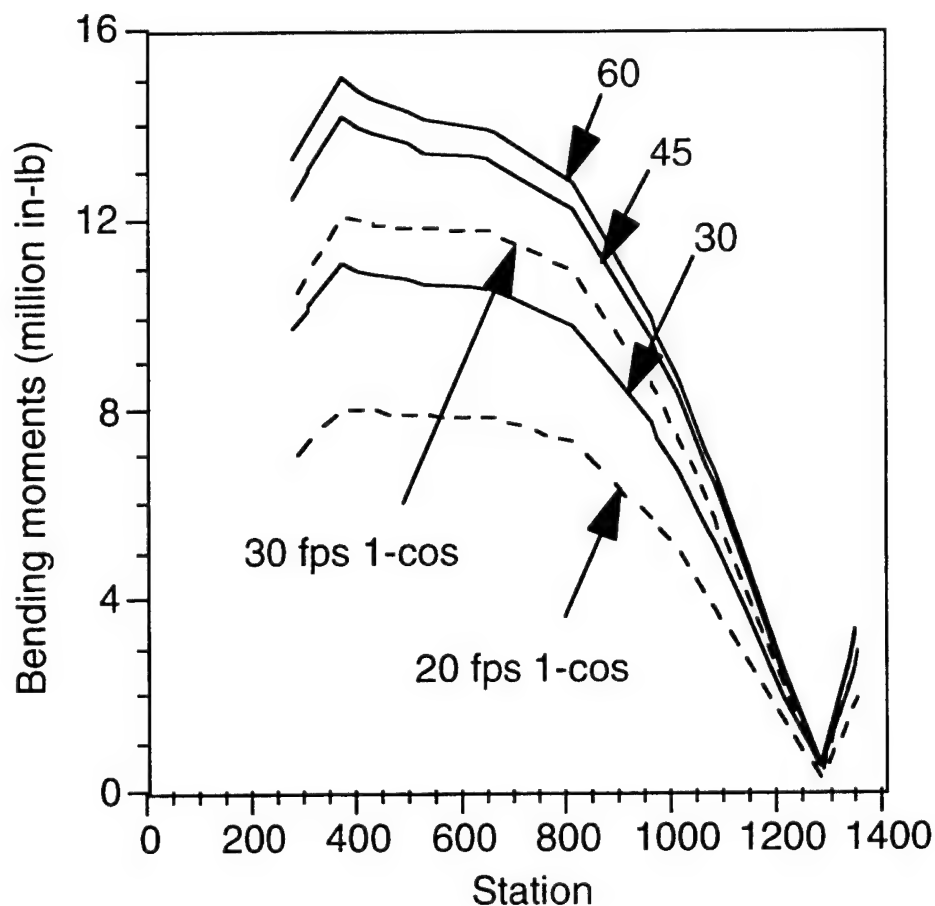
Figure 11. Heavy lift launch vehicle pitch bending moment comparison for stations
aft of the payload fairing. Lack-of-wind-persistence times of 30, 45, and 60
minutes. Western Range, 38000-44000-ft altitude band.

7.2 Effect of Altitude

Figures 12 and 13 present, for the medium and heavy lift launch vehicles, bending moments for
various altitude bands. The values were all calculated for the 30-min time period, which for the
vehicles under consideration is the shortest time that currently can be achieved between when a
profile is measured with balloons and placard calculations can be completed. To facilitate
comparisons between the various figures, the results for the one-minus-cosine synthetic profiles are
also included.

29
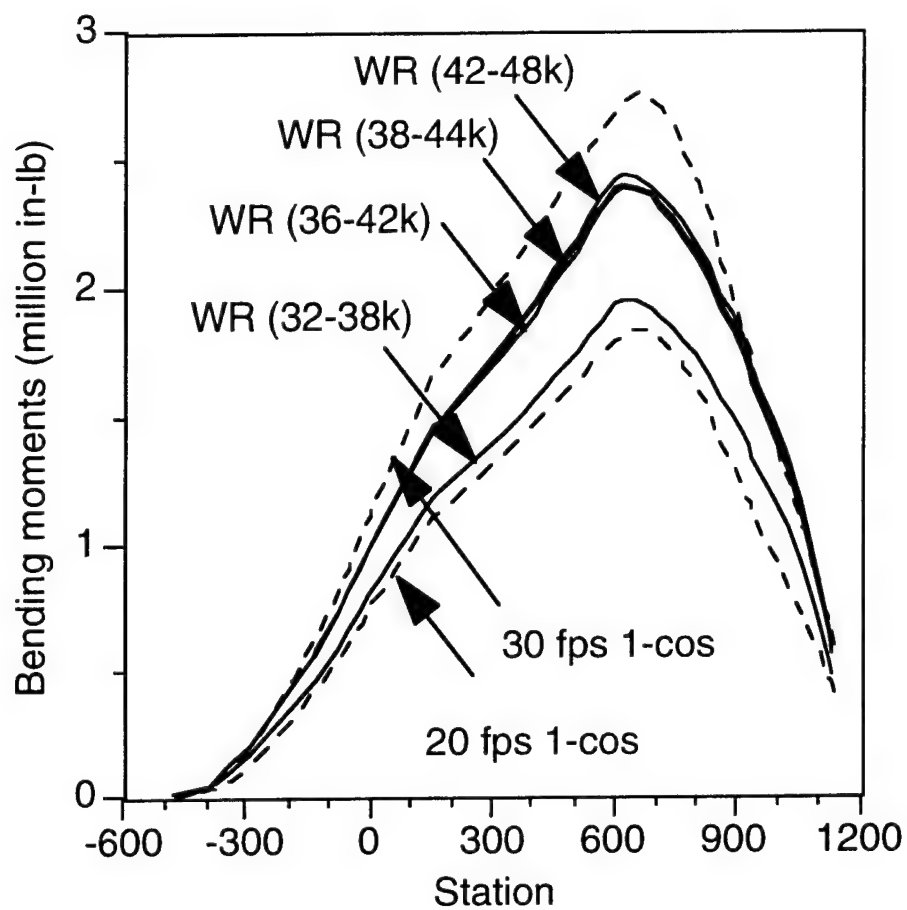
Figure 12. Medium lift launch vehicle pitch bending moment comparison showing the effects of altitude for the Western Range, lack-of-wind-persistence time of 30 min.
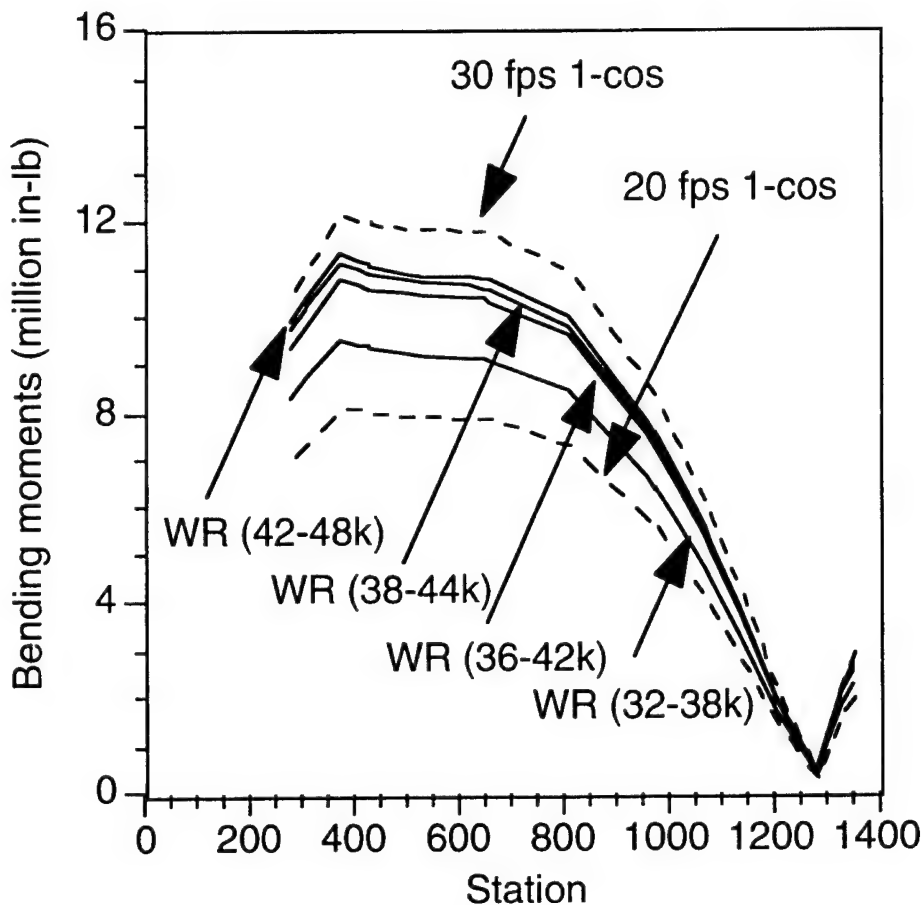
Figure 13. Heavy lift launch vehicle pitch bending moment comparison, for vehicle
stations aft of the payload fairing, showing the effects of altitude for the
Western Range, lack-of-wind-persistence time of 30 min.

As shown in these figures, there is a significant difference in gust loads obtained at the 42,000 to 48,000-ft altitude band and the 32,000 to 38,000-foot band. The results are consistent for both launch vehicles and both coasts, although the West Coast loads are higher. Also, whereas the 38,000 to 44,000-ft altitude band yields loads that are comparable to the 42,000 to 48,000-ft band on the West Coast, on the East Coast the lower band loads are lower.

It should be noted that, although not presented herein, results for the longer persistence time periods (45 min and 60 min) indicate that the 38,000 to 44,000-ft altitude band can provide loads that are comparable to those obtained at the higher altitude band with the shorter time period forcing functions. This observation is true for both the East and West coasts. Therefore, one must not conclude that the 42,000 to 48,000-ft altitude band is always going to provide the highest gust loads.

For the results presented herein, launch vehicle speed and dynamic pressure were kept constant in all analyses for all bands so that any load differences would be due solely to differences in turbulence.

31

Therefore, once vehicle speed and dynamic pressure changes with altitude are considered, the maximum turbulence/gust loads most likely will occur at a different altitude. Figures 14 and 15 summarize the maximum bending moment for each launch vehicle as a function of altitude. As indicated earlier, the West Coast loads are higher than those of the East Coast.
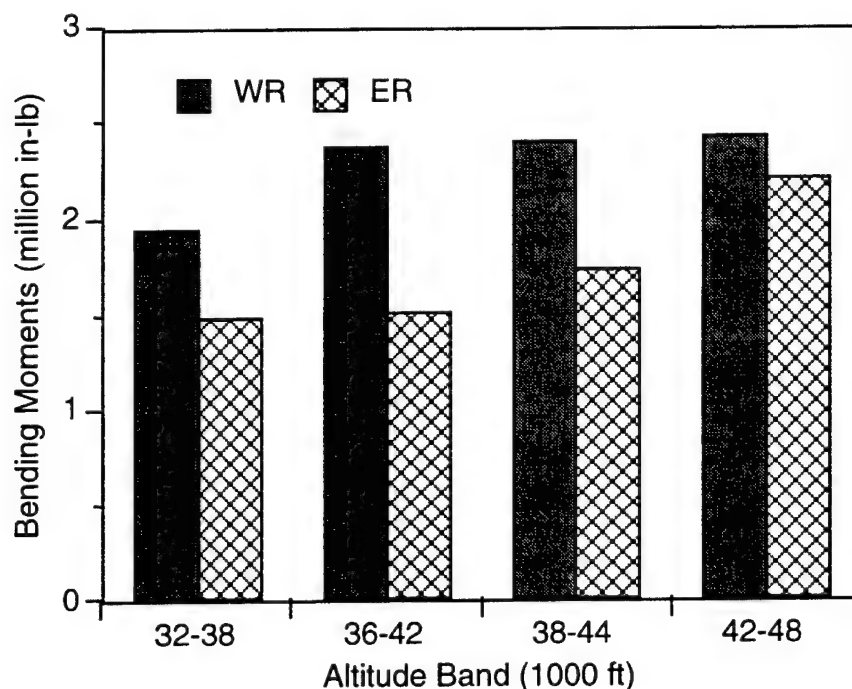
Figure 14. Medium lift launch vehicle peak pitch bending moment comparison. Loads obtained with 30-min forcing functions. Western Range loads are higher than for the Eastern Range. The launch vehicle speed and dynamic pressure were assumed to be the same in each analysis.
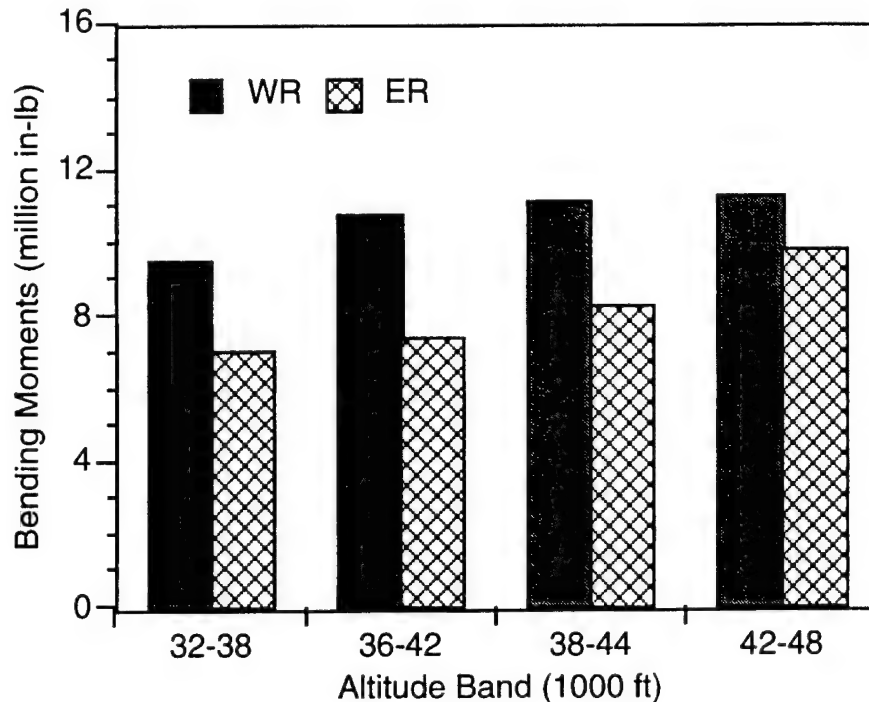
Figure 15. Heavy lift launch vehicle peak pitch bending moment comparison. Loads obtained with 30-min forcing functions. Western Range loads are higher than for the Eastern Range. The launch vehicle speed and dynamic pressure were assumed to be the same in each analysis.

7.3 Effect of Time of Year

Figures 16 and 17 compare loads obtained with forcing functions that were derived from winds measured only in the months of November through January, and February through April, to loads that correspond to the summer months of June, July and August, for the Eastern and Western Ranges, respectively. The annual average loads are also included. As can be seen, the turbulence in the November through April months yields loads that are significantly higher than in the summer months, and 10 percent higher than loads obtained when all 12 months are considered. Therefore, for design purposes, the higher winter month forcing functions should be used.

33
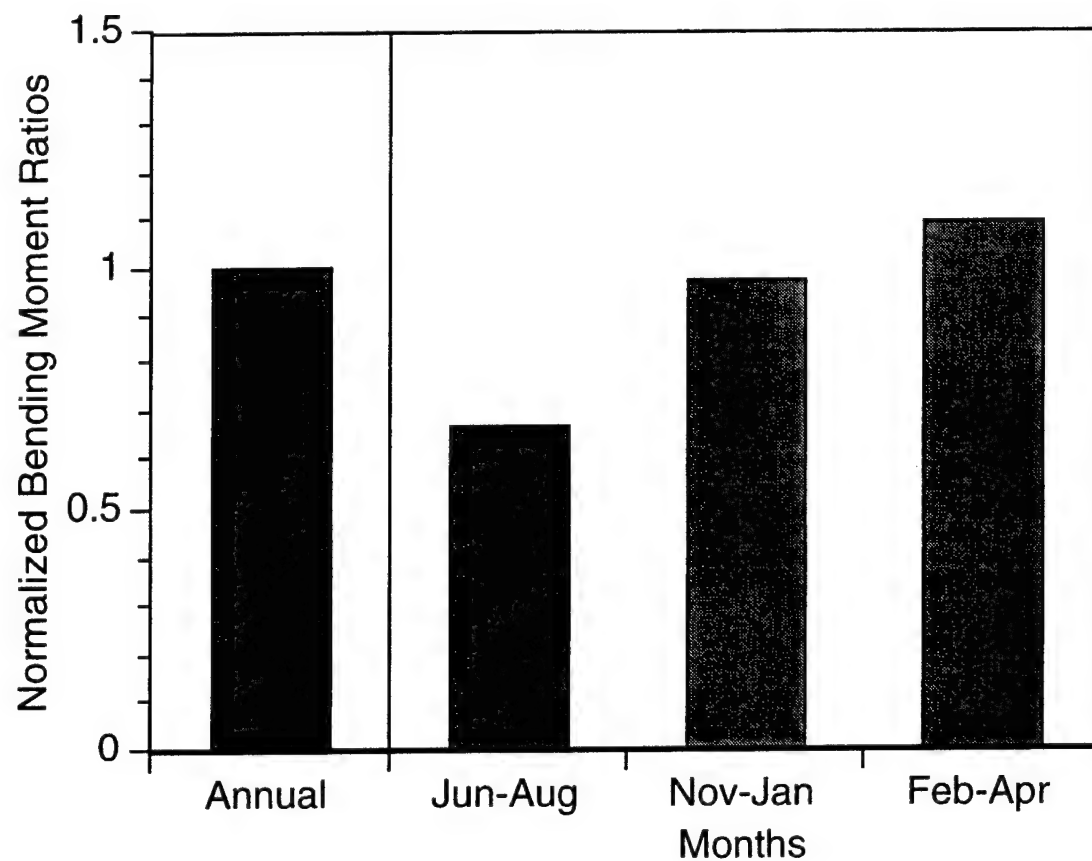
Figure 16. Heavy lift launch vehicle pitch bending moment comparison for the peak bending moment station showing the effects of season for the Eastern Range, 38000-44000-ft altitude, lack-of-wind-persistence time of 30 min. The bending moments were normalized with respect to the annual value. The months of February-April yield higher loads than the annual average.
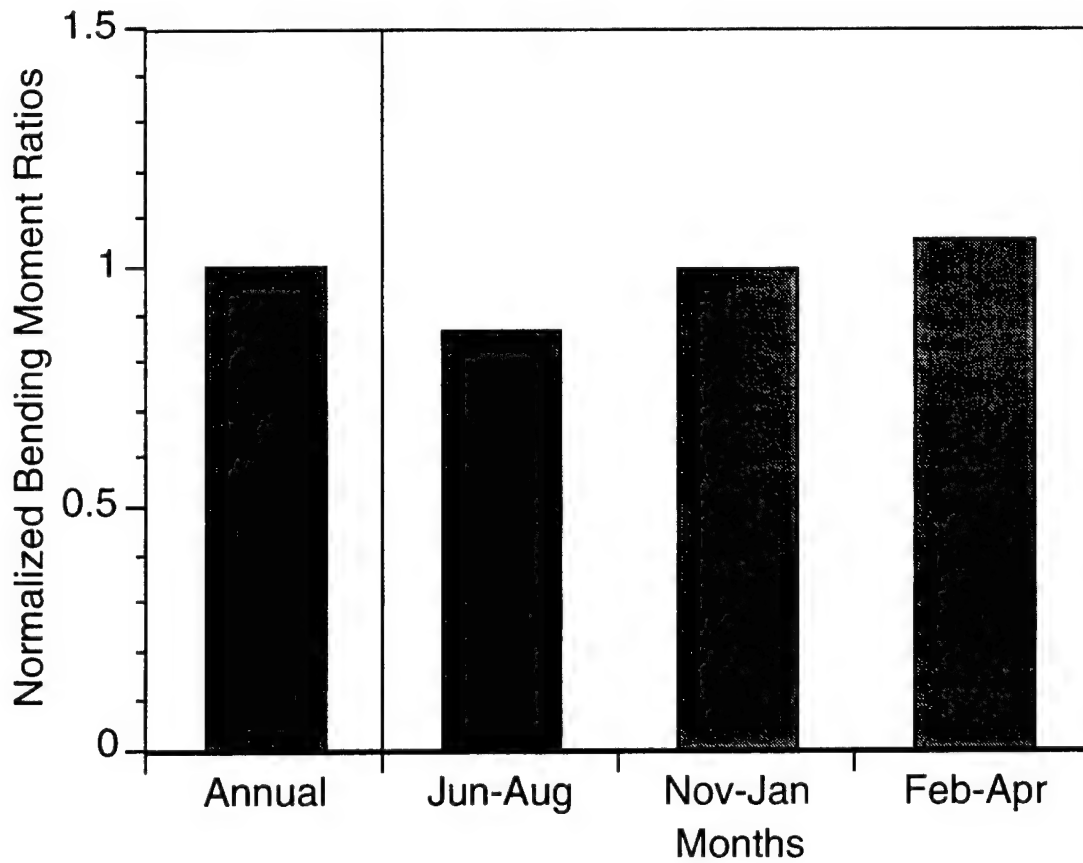
Figure 17. Heavy lift launch vehicle pitch bending moment comparison for the peak bending moment station showing the effects of season for the Western Range, 38000-44000-ft altitude, lack-of-wind-persistence time of 30 min. The bending moments were normalized with respect to the annual values. The months of February-April yield higher loads than the annual average.

8. Discussion

The Monte Carlo turbulence/gust loads analysis approach introduced in this paper has significant potential for more properly defining atmospheric turbulence/gust loads, and reducing unnecessary conservatism in day-of-launch placard calculations.[24] However, the results presented in this paper should only be extrapolated with caution. As discussed in Ref. 22, the turbulence/gust forcing functions are only appropriate for wavelengths greater than 500 ft. Critical spacecraft loads are often obtained with gust profiles that include shorter than 500-ft wavelengths. Therefore, at this time, the procedure presented here is not recommended for spacecraft gust load analysis, unless the critical loads are defined by wavelengths greater than 500 ft. Otherwise, the generally accepted approach of a one-minus-cosine profile with a 30-ft/sec amplitude, and appropriate reduction factors for short wavelengths should still be used.

9. Conclusions

A new Monte Carlo atmospheric flight gust loads analysis approach has been presented. The procedure uses forcing functions that were derived by extracting the short-duration, turbulent components of measured wind profiles. A large number of forcing functions were used in each analysis. The results were analyzed statistically to establish the 99.7 percent enclosure, 90 percent confidence level, load values. Results were presented for medium and heavy lift launch vehicles. Loads for various altitude bands, time of year, and for the Eastern and Western Range launch facilities in the United States were compared. Also, the Monte Carlo results were compared to a widely-used synthetic gust analysis approach.

A. Appendix

A.1 Synthetic Discrete Gust Profiles

In the early days, sharp-edged and linear-ramp type gust profiles were used (Refs. 18, 19). Other types of synthetic gusts that have been considered include the triangular, the trapezoidal, and the sine gusts (Ref. 4). The two most common synthetic gust profiles currently used today for launch vehicle loads analysis are the one-minus-cosine profile and the one-minus-cosine with a flattop profile (called the flattop profile). Parameters that can be varied with these synthetic gust profiles include the amplitude and wavelength; e.g., for the one-minus-cosine profile,

$$v(t) = \begin{cases} \dfrac{v_G}{2}(1 - \cos 2\pi f_G t) & \text{for } 0 \le t \le \dfrac{1}{f_G} \\ 0 & \text{for } \quad \dfrac{1}{f_G} < t \end{cases} \tag{A-1}$$

and where $f_G = v_{RW}/\lambda$ is the gust frequency, v_{RW} is the vehicle velocity, and λ is the gust wavelength. Figure A-1 shows the comparison between the one-minus-cosine profile and the one-minus-cosine with a flattop profile.
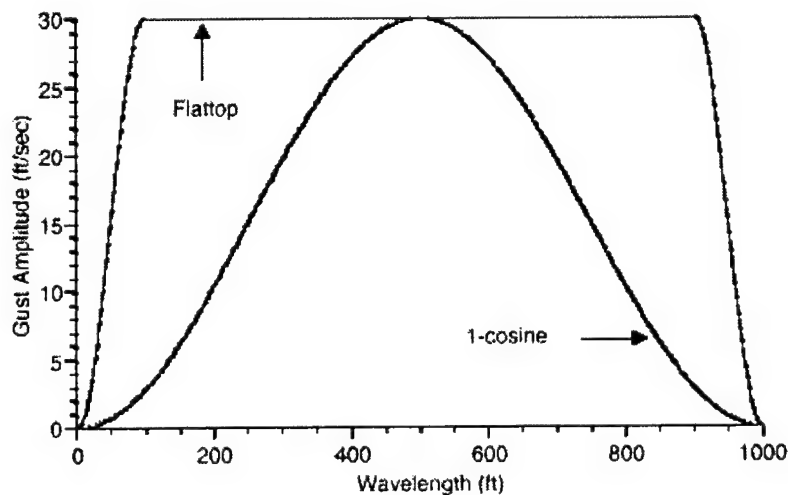

Figure A-1. Comparison of one minus cosine and the one-minus-cosine flattop profiles, for a wavelength of 1000 ft.

41

A.2 Gust Amplitude

The most widely used amplitude in launch vehicle loads analysis is 30 ft/sec, although some have suggested that 20 ft/sec might be a more appropriate value. This obviously will depend on how the other load contributors are established and combined on the day of launch, the time of year the vehicle flies, which coast, and the type of vehicle.

The 30-ft/sec gust amplitude has a long history, dating back to the early days of aviation.[25] However, even though a United States federal regulation included the sharp edge gust amplitude of 30 ft/sec as early as 1933 for aircraft gust loads analysis, it is not clear whether it was from this source that the 30-ft/sec, one-minus-cosine gust amplitude for launch vehicles was derived. In fact, a 50-ft/sec gust was specified for missile design as early as 1959.[15, 26]

Smith and Adelfang[27] theorized that the 30-ft/sec gust was derived from aircraft measurements taken in thunderstorms.[5, 6, 28] For launch vehicle gust considerations, NASA developed terrestrial climate guides, specifying a nine-meters/sec (approximately 30 ft/sec) flattop profile gust amplitude for design purposes.[16, 18, 29, 30] When combined with a severe wind shear, a reduction factor of 0.85 is recommended (Ref. 30). It should be noted, as discussed below, that the flattop profile yields higher loads than the pure one-minus-cosine profile.

A.3 Gust Wavelength

With the synthetic gust profiles, the wavelengths are selected to tune the gust to the coupled system fundamental modes of vibration. For heavy lift launch vehicles, gust wavelengths up to 1500 ft have been used. Gust wavelengths for medium lift launch vehicles have typically ranged from 800 ft to 1200 ft. Wavelengths as short as 200 ft, with appropriate attenuation factors, have been used for spacecraft gust loads analysis.

It must be noted that one should not draw a direct relationship between the wavelength of these synthetic profiles and the features of actual wind profiles. The intent of the synthetic profiles is not to duplicate actual wind features, but to induce with a relatively simple profile, loads that are equivalent to those that would be encountered when flying through the complex waveforms of severe turbulence.

A.4 Response Calculations

In the response calculations, the synthetic gust profile is assumed to act normal to the vehicle longitudinal axis. This results in a time-varying deviation from the relatively small vehicle angle of attack caused by the vehicle's motion through the atmosphere. It is also assumed that the launch vehicle is immersed in the gust profile instantaneously. Therefore, the gust velocity profile becomes a time-dependent modulation of the local angle of attack along the length of the vehicle. It is also assumed that the launch vehicle structural dynamic and aerodynamic properties do not vary significantly and, thus, a model with fixed parameters, appropriate for the altitude of interest, is used. The equations of motion must be augmented with an autopilot simulation that yields the proper engine side forces. Otherwise, incorrect loads will result.

Figure A-2 presents the bending moment diagrams for a medium lift launch vehicle that were obtained with the one-minus-cosine and the one-minus-cosine with flattop profiles. The wavelength used was 1000 ft, and the amplitude was 30 ft/sec for both profiles. As can be seen, the flattop profile yields loads that are up to 40 percent higher than the pure one-minus-cosine profile. Comparable results were obtained for the heavy lift launch vehicle. Figure A-3 shows for the heavy lift vehicle typical bending moment time histories obtained with the two profiles.
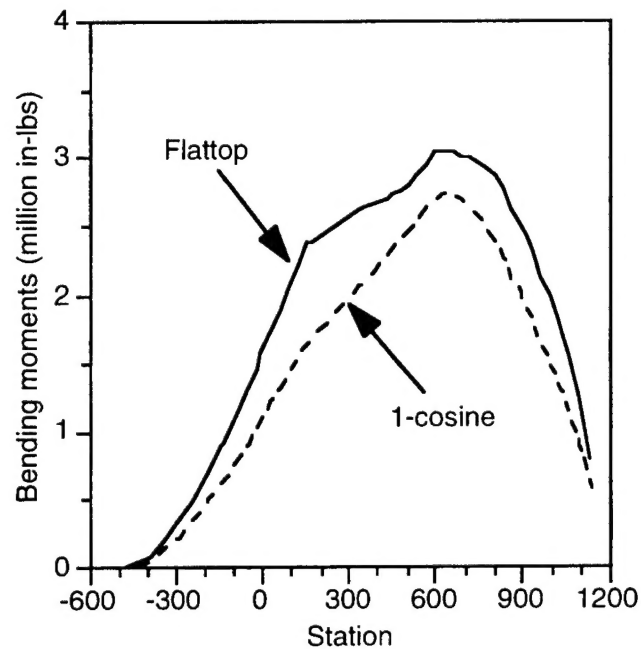
Figure A-2. Medium lift launch vehicle pitch bending moment comparison; a gust wavelength of 1000 ft and a gust amplitude of 30 ft/sec were used.
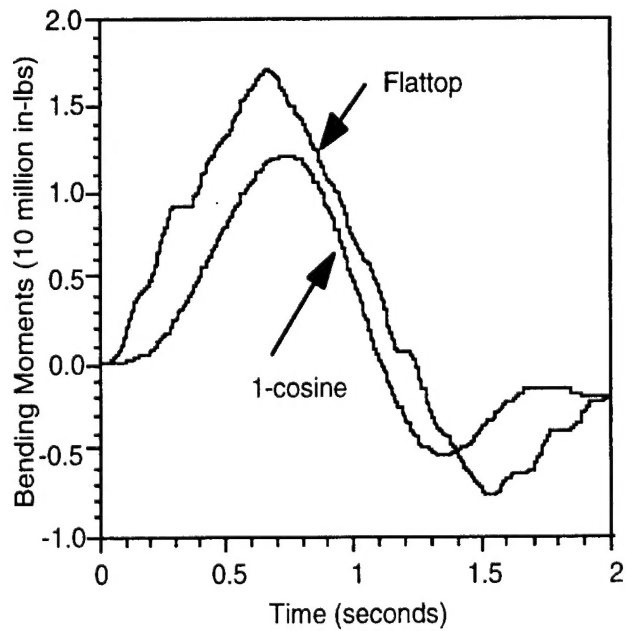

Figure A-3. Heavy lift launch vehicle pitch bending moment time history comparison for the peak bending moment station; a gust wavelength of 1500 ft and a

References

1. Lester, H. C., and Tolefson, H. B., "A Study of Launch-Vehicle Responses to Detailed Characteristics of the Wind Profile," J. Applied Meteorology, 3, 1964, pp. 491-498.

2. Scoggins, J. R., and Vaughan, W. W., "Problems of Atmospheric Wind Inputs for Missile and Space Vehicle Design," J. Spacecraft, 1, 2, 1964, pp. 181-184.

3. Ryan, R. S., Scoggins, J. R., and King, A., "Use of Wind Shears in the Design of Aerospace Vehicles," Journal of Spacecraft, 4, 11, 1967, pp. 1526-1532.

4. Zartarian, G., "Application of Atmospheric Turbulence Data in Design of Missiles & Booster Vehicles," AFCRL-69-0533, Jan. 1970.

5. Tolefson, H. B., "Preliminary Analysis of NACA Measurements of Atmospheric Turbulence Within a Thunderstorm - U. S. Weather Bureau Thunderstorm Project," NACA Tech. Note 1233, 1947.

6. Tolefson, H. B., "Summary of Derived Gust Velocities Obtained from Measurements Within Thunderstorms," NACA Tech. Note 1285, 1956.

7. Peckham, C. G., "A Summary of Atmospheric Turbulence Recorded by NATO Aircraft," NATO AGARD Report 586, 1971.

8. Van Gelder, P. A., "Derivation of Lateral and Vertical Gust Statistics from In-Flight Measurements," AIAA Paper 97-1214, 1997.

9. Adelfang, S. I., Ashburn, E. V., and Court, A., "A Study of Jimsphere Wind Profiles as Related to Space Vehicle Design and Operations," NASA Contractor Report CR-1204, 1968.

10. Adelfang, S. I., Court, A., Melvin, C. A., and Pazirandeh, M., "A Further Study of Jimsphere Wind Profiles as Related to Space Vehicle Design and Operations," NASA Contractor Report CR-1640, 1970.

11. Adelfang, S. I., and Court, A., "Jimsphere Wind and Turbulence Exceedance Statistics," NASA Contractor Report CR-2118, 1972.

12. Johnson, D. L., and Vaughan, W. W., "Sequential High-Resolution Wind Profile Measurements," NASA Tech. Paper 1354, Dec. 1978.

13. Smith, O. E., Adelfang, S. I., and Tubbs, J. D., "A Bivariate Gamma Probability Distribution with Application to Gust Modeling," NASA Tech. Memorandum 82483, 1982.

14. Treddenick, D. S., "A Comparison of Aircraft and Jimsphere Wind Measurements," Journal of Applied Meteorology, 10, 1971, pp. 309-312.

15. Hobbs, N. P., Criscione, E. S., Mazzola, L. L., and Frassinelli, G. J., "Development of Interim Wind, Wind Shear, and Gust Design Criteria for Vertically-Rising Vehicles," Wright Air Development Center Report 59-504, July 1959.

16. Daniels, G. E., editor, Terrestrial Environment (Climatic) Criteria Guidelines for Use in Aerospace Vehicle Development, 1973 Revision, NASA Tech. Memorandum X-64757, July 1973.

17. Kabe, A. M., "Design and Verification of Launch and Space Vehicle Structures," AIAA Paper 98-1718, 1998.

18. Daniels, G. E., "Natural Environment (Climatic) Criteria Guidelines for Use in MSFC Launch Vehicle Development," 1963 Rev., George Marshall Space Flight Center MTP-AERO-63-8, 1963.

19. Hoblit, F. M., *Gust Loads on Aircraft: Concepts and Applications*, AIAA Publications, 1988.

20. Smith, S. A., "Revised Gust Model," NASA MSFC ES44-(147-89), 1989.

21. Spiekermann, C. E., Sako, B. H., and Kabe, A. M., "Derivation of Non-Persistent Component of Winds for Atmospheric Flight Gust Loads Analysis," AIAA Paper 99-1250, 1999.

22. Sako, B. H., Kim, M. C., Kabe, A. M. and Yeung, W. K., "Derivation of Forcing Functions for Monte Carlo Atmospheric Gust Loads Analysis," AIAA Paper 99-1251, 1999.

23. Clark, J. B., Kim, M. C., Kabe, A. M., "Statistical Analysis of Atmospheric Flight Gust Loads Analysis Results," AIAA Paper 99-1253, 1999.

24. Kabe, A. M., Spiekermann, C. E., Kim, M. C., Lee, S. S., "A Refined and Less Conservative Day-of-Launch Atmospheric Flight Loads Analysis Approach," AIAA Paper 99-1255, 1999.

25. Murrow, H. N., Pratt, K. G., and Houbolt, J. C., "NACA/NASA Research Related to Evolution of U. S. Gust Design Criteria," AIAA Paper 89-1373-CP.

26. Mazzola, L. L., Hobbs, N. P., and Criscione, E. S., "Wind, Wind Shear, and Gust Design Criteria for Vertically-Rising Vehicles as Recommended on the Basis of Montgomery, AL., Wind Data," WADD-TR-61-99, Aug. 1962.

27. Smith, O. E., and Adelfang, S. I., "Wind Profile Models: Past, Present and Future for Aerospace Vehicle Ascent Design," AIAA Paper 98-1047.

28. Vaughan, W. W., "Analysis of Discrete Atmospheric Gust Velocity Data for Use in Missile Design and Performance Studies," Army Ballistic Missile Agency Report DA-TR-68-59, 1959.

29. Turner, R. E., and Hill, C. K., editors, "Terrestrial Environment (Climatic) Criteria Guidelines for Use in Aerospace Vehicle Development, 1982 Revision," NASA Tech. Memorandum 82473, 1982.

30. Johnson, D. L., editor, Terrestrial Environment (Climatic) Criteria Guidelines for Use in Aerospace Vehicle Development, 1993 Revision, NASA Tech. Memorandum 4511, 1993.